Author(s): Khattab, Sara, M.; Altowyan, Mezna Saleh; El-Faham, Ayman; Barakat, Assem; Haukka, Matti; Abu-Youssef, Morsy A. M.; Soliman, Saied M.

Title: A New Bromo-Mn(II) Complex with 1,3,5-Triazine Derivative: Synthesis, Crystal Structure, DFT and Biological Studies

Year: 2024

Version: Published version

inorganics

MDPI

Article

A New Bromo-Mn(II) Complex with 1,3,5-Triazine Derivative: Synthesis, Crystal Structure, DFT and Biological Studies

Sara M. Khattab [1,*], Mezna Saleh Altowyan [2], Ayman El-Faham [1,3], Assem Barakat [4,*], Matti Haukka [5], Morsy A. M. Abu-Youssef [1] and Saied M. Soliman [1]

[1] Department of Chemistry, Faculty of Science, Alexandria University, P.O. Box 426, Ibrahimia, Alexandria 21321, Egypt; ayman.elfaham@alexu.edu.eg or aymanel_faham@hotmail.com (A.E.-F.); morsy5@alexu.edu.eg (M.A.M.A.-Y.); saied1soliman@yahoo.com or saeed.soliman@alexu.edu.eg (S.M.S.)
[2] Department of Chemistry, College of Science, Princess Nourah bint Abdulrahman University, P.O. Box 84428, Riyadh 11671, Saudi Arabia; msaltowyan@pnu.edu.sa
[3] Department of Clinical Sciences, College of Medicine, Dar Al Uloom University, P.O. Box 45142, Riyadh 11512, Saudi Arabia
[4] Department of Chemistry, College of Science, King Saud University, P.O. Box 2455, Riyadh 11451, Saudi Arabia
[5] Department of Chemistry, University of Jyväskylä, P.O. Box 35, FI-40014 Jyväskylä, Finland; matti.o.haukka@jyu.fi
* Correspondence: saramahmoud@alexu.edu.eg or saramahmoud863@gmail.com (S.M.K.); ambarakat@ksu.edu.sa (A.B.)

Abstract: The crystal structure and topology analyses of a new bromo-Mn(II) complex with 2,4-*bis*(3,5dimethyl-1*H*-pyrazol-1-yl)-6-methoxy-1,3,5-triazine (MBPT) were reported. Its structure was confirmed using single-crystal X-ray diffraction to create the formula $[Mn(MBPT)Br(H_2O)_2]ClO_4$. Its crystal system was monoclinic and its space group was $p2_1$. The Mn(II) was coordinated with MBPT as a *NNN*-pincer ligand, with one bromide ion in the equatorial plane. The two axial terminals were occupied by two *trans* water molecules. H. . .H, N. . .H, Br. . .H, C. . .H and O. . .H were the predominant intermolecular contacts, while Br. . .H, O. . .H and C. . .O were the significant contacts based on Hirshfeld analysis. Moreover, anion–π interaction was found between C(*s*-triazine) and O(perchlorate). This complex had better antioxidant activity than the free ligand (MBPT). In addition, the cytotoxicity of the $[Mn(MBPT)Br(H_2O)_2]ClO_4$ complex showed better results against HepG-2 and MCF-7 cells, recording IC_{50} values of 31.11 ± 2.04 and 50.05 ± 2.16 µM, respectively, compared to the free ligand (IC_{50} = 671.44 ± 21.41 and 1113.55 ± 29.77 µM). In comparison to *cis*-platin as a reference drug, the IC_{50} values were 63 and 80 µM, respectively, which indicated the promising anticancer activity of the studied compound against both cell lines. In terms of the safety of normal cells, the Mn(II) complex recorded a high IC_{50} value of 359.10 ± 8.72 µM against the WI-38 non-cancerous cell line. The complex showed better activity towards *Staphylococcus aureus*, *Bacillus subtilis*, and *Proteus vulgaris* relative to the free MBPT, but had low to moderate activity compared to Gentamycin as an antibacterial positive control.

Keywords: X-ray crystal structure; *bis*-pyrazol-s-triazine; pincer Mn(II) complex; Hirshfeld; biological studies

Citation: Khattab, S.M.; Altowyan, M.S.; El-Faham, A.; Barakat, A.; Haukka, M.; Abu-Youssef, M.A.M.; Soliman, S.M. A New Bromo-Mn(II) Complex with 1,3,5-Triazine Derivative: Synthesis, Crystal Structure, DFT and Biological Studies. *Inorganics* **2024**, *12*, 284. https://doi.org/10.3390/inorganics12110284

Academic Editor: Marius Andruh

Received: 3 October 2024
Revised: 28 October 2024
Accepted: 29 October 2024
Published: 31 October 2024

1. Introduction

Manganese is regarded as one of the most important micro-nutrients in the human body [1]. It is involved in many vital processes inside biological systems such as the synthesis and activation of several enzymes (e.g., redox or hydrolytic transformations), the metabolism of carbohydrates and lipids, and assistance in the production of proteins and some vitamins (in particular, C and B) [2–4]. For the past few decades, complexes of manganese gained special attention due to their exceptional role in biomedical applications and the ability of their ions to have different oxidation states [5,6]. For instance, various

Mn(II) complexes can be used as contrast-enhanced MRI agents [7–9], and in manganese superoxide dismutase (MnSOD) mimetics, which are responsible for the reduction in reactive oxygen species (ROS) that cause oxidative stress inside mitochondria [10–14]. The overall physiological roles of manganese help in improving human immunity [4]. The increased selectivity of the manganese element in forming high-stable complexes with certain organic ligands introduces extra privilege for it among the other available first row transition metal ions (e.g., Zn, Fe, and Cu) [1]. The ligands that are responsible for manganese chelation are known as sequestering agents, which prevent overload Mn(II) accumulation [15]. Moreover, manganese complexes are attracting current focus due to their low in vivo toxicity, and their remarkable antimicrobial and anticancer activities, which make them good candidates for different infection diseases and cancer treatments instead of platinum-based chemotherapeutic drugs such as *cis*-platin [16,17].

s-Triazine and its derivatives have very interesting and promising potential due to their presence in many naturally occurring substances and their affordability. Also, they are common in various commercially available drugs that are used as anticancer, antimicrobial, antiviral and anti-inflammatory agents [18–20]. In recent years, several studies were performed to introduce active heterocyclic add-ons to the *s*-triazine nucleus to obtain more potent compounds [19]. In addition, pyrazoles were investigated as important heterocyclic analogs due to possessing remarkable bioactivities that are like that of *s*-triazines [21–24]. For example, novel derivatives of mono- and *bis*(dimethylpyrazolyl)-*s*-triazine were synthesized and tested on several cancerous cell lines (e.g., breast cancer, colon cancer, and liver cancer cell lines) that showed very promising results [21]. 2,4-*Bis*(3,5-dimethyl-1*H*-pyrazol-1-yl)-6-methoxy-1,3,5-triazine (MBPT, Figure 1) was an interesting *N,N,N-pincer* ligand. This interesting chelator is capable of coordinating different metal ions, leading to many coordination compounds with interesting biological activities [25–28].

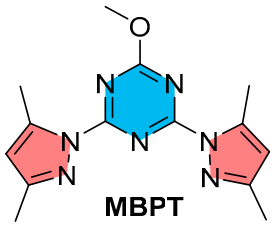

Figure 1. Structure of MBPT.

The previously reported Ni(II), Zn(II) and Co(II) complexes with this ligand were found to have interesting molecular and supramolecular structures in addition to their diverse biological activity as antimicrobial and anticancer agents where the nature of the metal ion, coordinating ligand and anionic groups, affected their biological potentials [25–28]. In continuation of our previous studies, herein, we synthesized a new bromo Mn(II)–MBPT complex, exploring its antimicrobial, antioxidant and anticancer properties. In this regard, its cytotoxicity was examined against three cancerous cells (A-549, MCF-7 and HepG-2). In addition, its crystal structure was reported for the first time in combination with its Hirshfeld analysis.

2. Results and Discussion

2.1. Synthesis and Characterization

The self-assembly of manganese perchlorate, MBPT and KBr in an ethanol–water mixture as solvent afforded the bromo Mn(II) pincer complex a good yield. The weak coordinating ability of the perchlorate anion enabled the incorporation of the bromide ion into the coordination sphere of the complex (Scheme 1). Its molecular formula was assigned to be $[Mn(MBPT)Br(H_2O)_2]ClO_4$ based on the X-ray diffraction of a single crystal. The FTIR spectra provided the essential evidence on the complexation between Mn(II) and MBPT. Two characteristic bands were observed at 1541 and 1614 cm^{-1} for

the $[Mn(MBPT)Br(H_2O)_2]ClO_4$ complex, which were attributed to the $\upsilon_{(C=N)}$ stretching vibration mode of the pyrazole rings and the triazine moiety, respectively [29,30]. The respective values for MBPT were 1561 and 1598 cm^{-1} [25]. The sharp peak at 629 cm^{-1} could be related to $\delta_{(ClO)}$ asymmetric bending (υ_4), while the broad triple split band at 1037, 1083 and 1134 cm^{-1} could be related to the $\upsilon_{(ClO)}$ asymmetric stretching (υ_3) bands (Figure S1) [31–33].

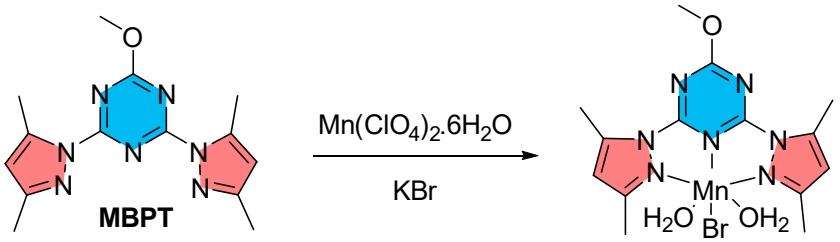

Scheme 1. Synthesis of $[Mn(MBPT)Br(H_2O)_2]ClO_4$.

2.2. Crystal Structure Description

The structural aspects of $[Mn(MBPT)Br(H_2O)_2]ClO_4$ were investigated via single-crystal X-ray diffraction measurement. The new complex had the monomeric formula $[Mn(MBPT)Br(H_2O)_2]ClO_4$ as an asymmetric unit (Figure 2). The complex $[Mn(MBPT)Br(H_2O)_2]ClO_4$ was crystallized in the monoclinic crystal system, the $P2_1$ space group and Z = 4.

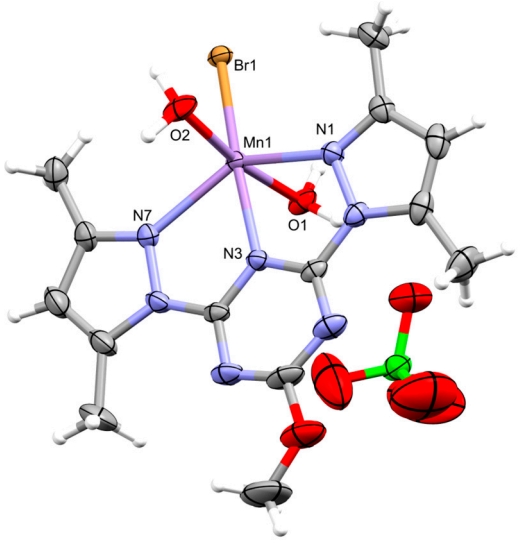

Figure 2. The asymmetric unit structure and atomic numbering of the $[Mn(MBPT)Br(H_2O)_2]ClO_4$ complex. Thermal ellipsoids were drawn at the 30% probability level.

The cationic coordination sphere of this complex comprised hexa-coordinated Mn(II) with one MBPT as a *N,N,N*-pincer ligand, one bromide ion and two H_2O molecules *trans* to one another. The outer sphere had one perchlorate ion (Figure 2). An analysis of the bond distances around the Mn(II) central atom showed that the two axial Mn1-O1 (2.196(4) Å) and Mn1-O2 (2.155(5) Å) bonds were the shortest, while the Mn1-Br1 was the longest bond (2.6018(10) Å). The manganese to nitrogen distances were variable, where Mn1-N3 (2.221(5) Å), which belongs to *s*-triazine ring, was significantly shorter than the Mn1-N1 (2.304(5) Å) and the Mn1-N7 (2.296(5) Å) of the two pyrazoles rings [25]. The two bite angles N3-Mn1-N1and N3-Mn1-N7 of the tridentate ligand were 69.39(18) and 69.23(19)°, while the angle between the two Mn-N bonds of the *trans* pyrazole moieties (N7-Mn1-N1) was 137.64(19)°. The angles between the two axial water molecules and the bromide ion were

determined to be 85.57(12) and 88.90(14)° for O1-Mn1-Br1 and O2-Mn1-Br1, respectively, while the *trans* bond angle O2-Mn1-O1 was 171.7(2)° (Table 1). Hence, the coordination geometry around Mn(II) was distorted octahedra.

Table 1. Bond distances and angles (Å, °) of the coordination sphere in $[Mn(MBPT)Br(H_2O)_2]ClO_4$.

Bond Distances			
Mn1-O1	2.196(4)	Mn1-N7	2.296(5)
Mn1-O2	2.155(5)	Cl1-O5	1.398(8)
Mn1-Br1	2.6018(10)	Cl1-O4	1.258(9)
Mn1-N1	2.304(5)	Cl1-O6	1.343(10)
Mn1-N3	2.221(5)	Cl-O7	1.389(13)
Bond Angles			
O1-Mn1-Br1	85.57(12)	O2-Mn1-N3	101.70(19)
O1-Mn1-N1	87.42(19)	O2-Mn1-N7	90.8(2)
O1-Mn1-N3	84.06(17)	N3-Mn1-Br1	169.27(13)
O1-Mn1-N7	96.95(18)	N3-Mn1-N1	69.39(18)
N1-Mn1-Br1	112.90(13)	N3-Mn1-N7	69.23(19)
O2-Mn1-O1	171.7(2)	N7-Mn1-Br1	109.45(14)
O2-Mn1-Br1	88.90(14)	N7-Mn1-N1	137.64(19)
O2-Mn1-N1	89.0(2)		

Intermolecular H-bonds and anion–π stacking were the driving forces behind the packing of the $[Mn(MBPT)Br(H_2O)_2]ClO_4$ complex in the 3D structure where these supramolecular interactions were clearly shown in Figure 3. Hydrogen bonding interactions including the O-H. . .O and O-H. . .Br interactions are depicted in Table 2. The hydrogen acceptor distances for the O1-H1A. . .O5 and O2-H2A. . .O5 hydrogen bonds were 2.10 and 2.48(17) Å, respectively, while the related donor-to-acceptor distances were 2.876(10) and 3.047(12) Å, respectively. The O2-H2B. . .Br1 and O1-H1B. . .Br1 hydrogen bonds had oxygen-to-Br distances of 3.314(5) and 3.338(4) Å, respectively. On a worthy note, the extensive intermolecular hydrogen bonding system (O-H. . .O) generated the differences in the Cl-O bond lengths (1.258(9)–1.398(8) Å; Table 1) which explains the complicated character of the band assigned to the υ_3 vibration mode of the perchlorate group in the IR spectrum [34].

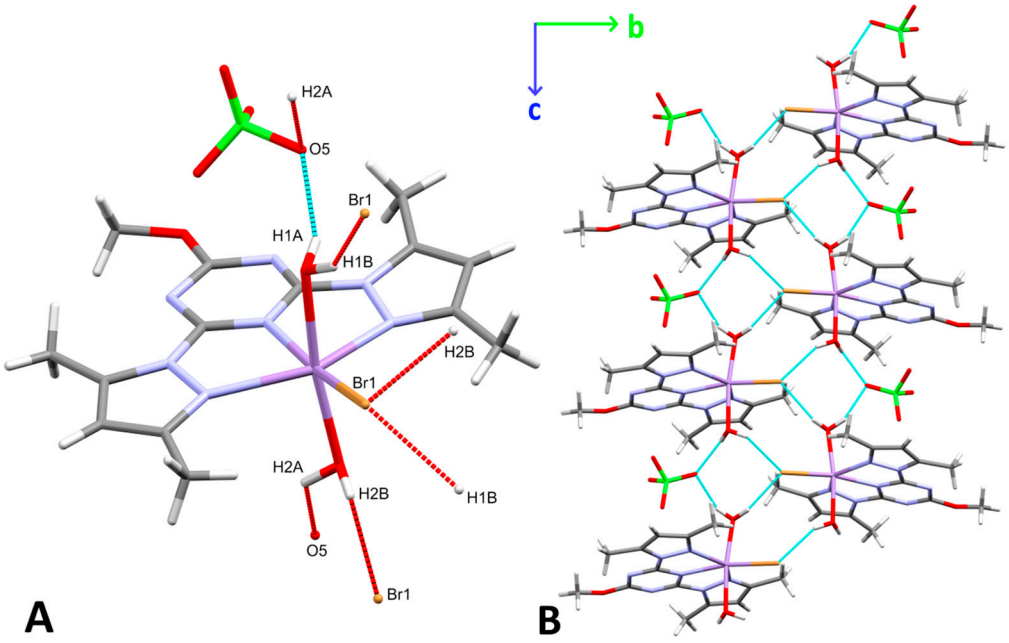

Figure 3. The significant H-bond contacts (**A**), and the H-bond packing along the *bc* plane (**B**).

Table 2. H-bond geometric parameters of $[Mn(MBPT)Br(H_2O)_2]ClO_4$.

D-H...A	D-H(Å)	H...A(Å)	D...A(Å)	D-H...A(°)	Symm. Code
O1-H1A...O5	0.85	2.10	2.876(10)	152.3	
O1-H1B...Br1	0.85	2.58	3.338(4)	148.4	+x, 1/2 − y, 1/2 + z
O2-H2A...O5	0.890(10)	2.48(17)	3.047(12)	122(15)	+x, +y, −1 + z
O2-H2B...Br1	0.888(10)	2.45(2)	3.314(5)	164(6)	+x, 1/2 − y, −1/2 + z

In addition, anion–π interactions were detected in the crystal structure of the $[Mn(MBPT)Br(H_2O)_2]ClO_4$ complex (Figure 4). Three significant anion–π contacts were recognized between the carbon atoms of the *s*-triazine core and the oxygen atoms of the perchlorate anion. The C8...O4[a] (3.02(2) Å; Symm. code: x,y,−1 + z), C8...O6 (3.20(1) Å) and C7...O6 (3.18(2) Å) short contacts confirmed the presence of anion–π stacking interaction.

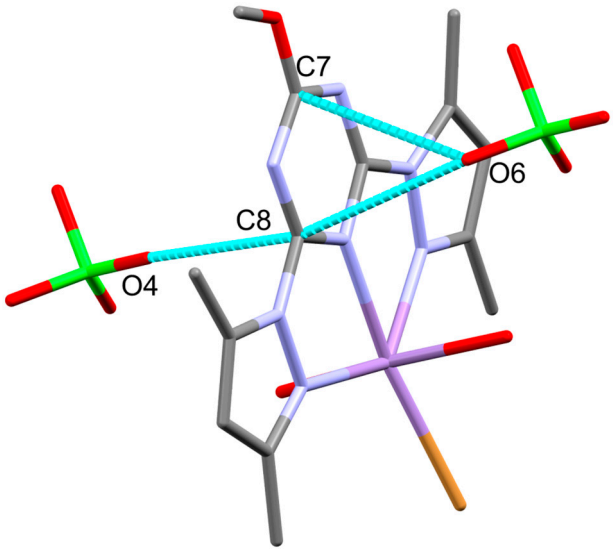

Figure 4. Anion–π interactions in $[Mn(MBPT)Br(H_2O)_2]ClO_4$.

2.3. Hirshfeld Surface Analysis

A Hirshfeld surface analysis was used to further investigate the most significant intermolecular interactions that control the molecular packing of $[Mn(MBPT)Br(H_2O)_2]ClO_4$. The leading contacts were indicated as red circles with shorter distances, while the blue regions had longer distances and the white regions had equal distances compared to the sum of the van der Waals radii of the interacting atoms. The studied surface was visualized by d_{norm}, shape index and curvedness functions (Figure 5). The d_{norm} map was in a color range from 0.1 to 1.0; the strong close contacts are given in Table 3.

Table 3. Close contacts and their distances for the $[Mn(MBPT)Br(H_2O)_2]ClO_4$ complex based on Hirshfeld calculations.

Contact	Contact Distance (Å)	Contact	Contact Distance (Å)
Br1...H1B	2.472	H2A...O5	2.437
Br1...H2B	2.360	H11...O7	2.545
Br1...H3	2.843	C7...O6	3.182
H1A...O5	1.980	C8...O6	3.196
H2A...O4	2.533	C8...O4	3.022

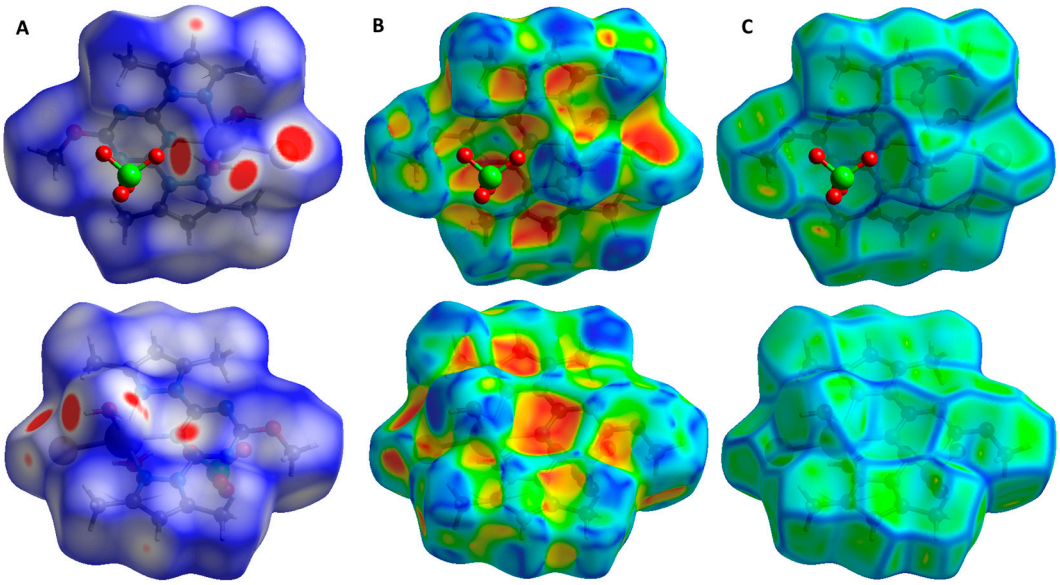

Figure 5. Hirshfeld surfaces illustrated with d_{norm} (**A**), shape index (**B**), and curvedness (**C**) maps in two different views.

The predominant interactions in the crystal structure were the H. . .H, O. . .H, Br. . .H, C. . .H and N. . .H, which participated by 42.8, 23.4, 10.6, 9.0 and 7.3%, respectively (Figure 6). The anion–π interaction generally existed between C(*s*-triazine) and O(perchlorate), which contributed to 2.4% of the total interactions. Moreover, C8. . .O4 was the shortest (3.02(2) Å) while the other two anion–π interactions of C7. . .O6 and C8. . .O6 were almost equal (3.18 and 3.20 Å, respectively).

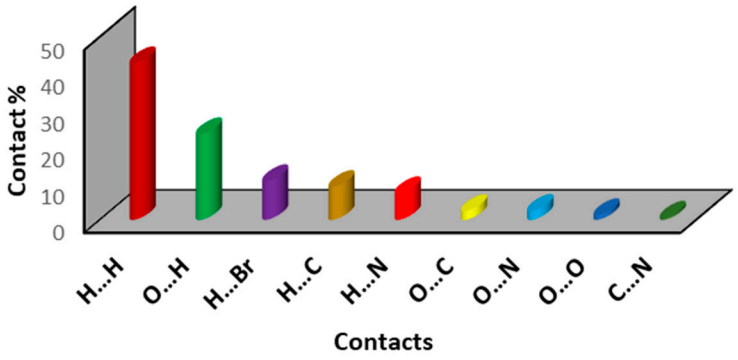

Figure 6. The contributions of intermolecular interactions for the $[Mn(MBPT)Br(H_2O)_2]ClO_4$ complex.

The Br. . .H, O. . .H and C. . .O contacts appeared in the d_{norm} map as red regions, indicating their importance for molecular packing. The spikes in the fingerprint plots emphasized the most important contacts while the area of the fingerprint plot represented the contacts' contribution (Figure 7). As clearly seen from Table 3, the H2B. . .Br1, H1A. . .O5 and C8. . .O4 contacts had the shortest distances of 2.360, 1.980 and 3.022 Å, respectively. It is worthy to note that the two spikes of the O. . .H/H. . .O contacts were not symmetric, indicating that the surface was more likely to be a hydrogen bond donor for this type of intermolecular interaction. On the other hand, the two spikes of the Br. . .H/H. . .Br contacts were looking symmetric, indicating that the surface was acting as both a hydrogen bond donor and an acceptor with respect to the Br. . .H interactions.

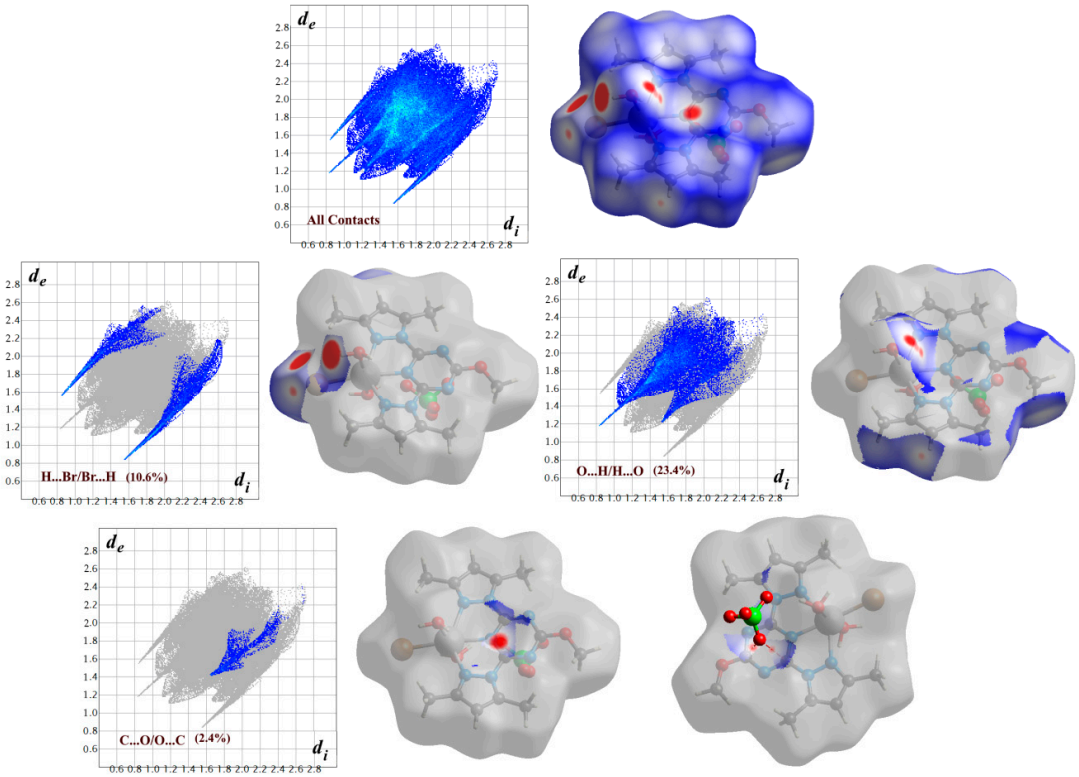

Figure 7. The d_{norm} maps of the close contacts and their corresponding 2D fingerprints.

2.4. Metal Affinity Study

A comparative discussion illustrating the affinities of some divalent metal ions [26–28,35] towards the MBPT ligand was introduced. The interaction energies were calculated for the cationic complex units $[M\text{-}MBPT]^{2+}$, which revealed that Mn(II) in the $[Mn(MBPT)Br(H_2O)_2]ClO_4$ complex had the lowest affinity towards the MBPT ligand. The main factors that affected the affinity of MBPT towards the M(II) ion were: (1) the metal ion charge, (2) the coordinating anionic or neutral ligand groups and (3) the metal ion size. Since all the studied systems had divalent metal ions, the two last parameters were the most effective in determining the metal affinity of MBPT. It is obvious that the largest M(II)-MBPT affinity was detected for the M(II) complexes that had no coordinating anion and a small size metal ion (Ni(II)), as found in complexes **7** and **8** (Table 4). The replacement of one aqua molecule via chloride as found in complex **6** led to the lowering of the metal affinity to 345.3815 kcal/mol. For the related Co(II) complexes (**4** and **5**), the Co(II)-MBPT affinities were less compared to **8** and **7**, respectively, which could be attributed to the difference in the metal ion size.

Table 4. The M(II)-MBPT affinity of the studied complexes [a].

Complex	$[M(II)\text{-}L]^{2+}$	MBPT	M(II)	E_{int} [b]
$[Mn(MBPT)Br(H_2O)_2]ClO_4$; **1**	−1105.0853	−1001.6449	−103.0413	−250.4392
$[Co(MBPT)(H_2O)_2Cl]Cl$; **2**	−1146.1391	−1001.5828	−144.0981	−287.5251
$[Co(MBPT)(NO_3)_2]$; **3**	−1146.2080	−1001.6447	−144.0981	−291.9177
$[Co(MBPT)(H_2O)_3](ClO_4)_2 . H_2O$; **4**	−1146.2086	−1001.6433	−144.0981	−293.1727
$[Co(MBPT)(H_2O)_3](NO_3)_2.H_2O$; **5**	−1146.2108	−1001.6463	−144.0981	−292.6707
$[Ni(MBPT)(H_2O)_2\ Cl]Cl$; **6**	−1170.4113	−1001.6402	−168.2207	−345.3815
$[Ni(MBPT)(H_2O)_3](NO_3)_2.1/2\ H_2O$; **7**	−1170.4110	−1001.6221	−168.2207	−356.5826
$[Ni(MBPT)(H_2O)_3](ClO_4)_2 . H_2O$; **8**	−1170.4284	−1001.6424	−168.2207	−354.7314
$[Zn(MBPT)(H_2O)Cl]\ ClO_4$; **9**	−1066.6811	−1001.6460	−64.5754	−288.4663
$[Zn(MBPT)(NO_3)_2]$; **10**	−1066.6785	−1001.6447	−64.5754	−287.6506

[a] All values in a.u. except E_{int} in kcal/mol; [b] $E_{int} = E_{Complex} - (E_{Metal} + E_{Ligand})$.

2.5. Antioxidant Activity

1,1-Diphenyl-2-picrylhydrazyl (DPPH) is a standard stable organic radical, which is used in the quantitative assay of reactive oxygen species (ROS). Free radical scavenging is helpful to minimize the oxidative damage caused by ROS to the human body [36]. The antioxidant activities of $[Mn(MBPT)Br(H_2O)_2]ClO_4$ and the ligand together with ascorbic acid were determined on the basis of the free radical scavenging ability of DPPH. The inhibition percents indicated that the Mn(II) complex was stronger than the ligand as a free radical scavenger and antioxidant, but weaker when compared to the ascorbic acid as a standard. The values of the calculated IC_{50} of the Mn(II) complex and vitamin C were 824.97 ± 41.71 and 57.97 ± 4.37 μM, respectively, while the ligand showed almost no antioxidant activity under the same experimental conditions (Figure S2). The antioxidant activity of the previously studied structurally related metal(II) complexes were compared to that for the $[Mn(MBPT)Br(H_2O)_2]ClO_4$ complex. The $[Zn(MBPT)(NCS)_2]$ and $[Zn(MBPT)(Br)_2]$ complexes had IC_{50} values of 156.996 ± 8.5 and 675.286 ± 38.59 μM, respectively [27], which were generally better antioxidants than the $[Mn(MBPT)Br(H_2O)_2]ClO_4$ complex.

2.6. Antimicrobial Assay

Antibacterial screening of the $[Mn(MBPT)Br(H_2O)_2]ClO_4$ complex was examined on two Gram-positive bacteria *Staphylococcus aureus* (RCMB010010) and *Bacillus subtilis* RCMB 015 (1) NRRL B-543, and two Gram-negative bacteria, namely, *Escherichia coli* ATCC 25922 and *Proteus vulgaris* RCMB 004 (1) ATCC 13315. The agar–well diffusion technique was used for the antimicrobial assay [37], where all the samples were tested at 10 mg/mL concentration and compared with the Gentamycin antibiotic as a positive control. The results showed the enhanced activity of the Mn(II) complex against all the tested strains (except *E. coli*) compared to the free ligand. The latter showed no activity against the variety of pathogens [27], which corroborates that the enhanced activity of the complex could be related to its lipophilic character [38]. The studied Mn(II) complex was active against *S. aureus* (14 mm), *B. subtilis* (19 mm), and *P. vulgaris* (16 mm). For Gentamycin, the respective values were 24, 26 and 25 mm. Hence, the antibacterial activity of the Mn(II) could be considered good with respect to the standard antibiotic. Further, antifungal scanning showed no activity against the *A. fumigatus* and *C. albicans* fungal species (Table S1).

2.7. Safety Assay

An in vitro viability assessment was made to figure out the safety pattern of the $[Mn(MBPT)Br(H_2O)_2]ClO_4$ complex and the MBPT ligand, where variable concentrations were prepared to test the safety profile of both the samples against WI-38 (the human lung fibroblast non-cancerous cell line, provided by ATCC, Rockville, MD). Using an MTT assay, IC_{50} values were determined to be 359.10 ± 8.72 and 1320.22 ± 31.64 μM for $[Mn(MBPT)Br(H_2O)_2]ClO_4$ and MBPT, respectively (Figure S3). Hence, the complex showed higher cytotoxicity than the free ligand. Regardless, the IC_{50} value of the Mn(II) complex was considered high and indicated its relatively higher in vitro safety pattern towards the non-cancerous cell line.

2.8. Cytotoxicity Assay

The in vitro anticancer activities of $[Mn(MBPT)Br(H_2O)_2]ClO_4$ and the free ligand were studied against the A-549 (lung carcinoma), MCF-7 (breast cancer), HeLa(Cervical cancer), and HepG-2 (Human liver cancer) cell lines (ATCC, Rockville, MD) at different concentrations by using an MTT assay. The cytotoxicity results shown in Figure 8 indicated that the Mn(II) complex markedly inhibited all the selected cancerous cell lines to different extents.

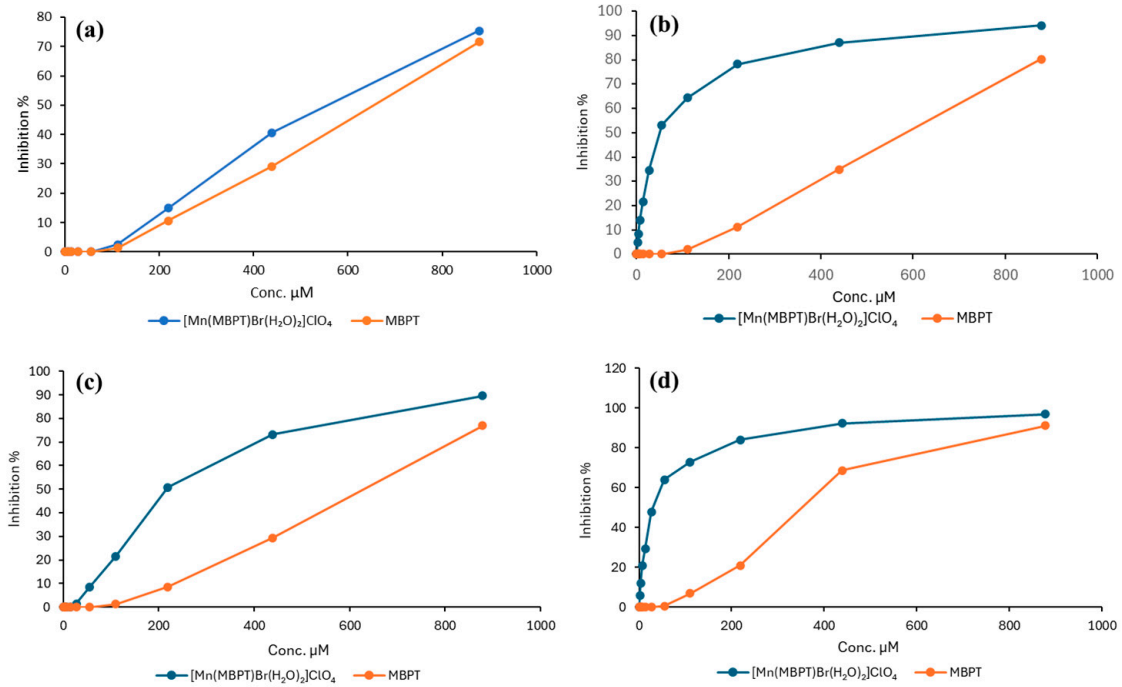

Figure 8. Anticancer activities of the $[Mn(MBPT)Br(H_2O)_2]ClO_4$ complex and the free ligand (MBPT) on the A-549 (**a**), MCF-7 (**b**), HeLa (**c**), and HepG-2 cell lines (**d**).

The maximum percentages of inhibition on A-549 after treatment with the Mn(II) complex and the ligand were 75.29 and 71.61%, respectively, and the IC_{50} values were 557.75 ± 20.15 and 1245.41 ± 45.57µM, respectively. The inhibition percentages of the complex and the ligand on MCF-7 were 94.17 and 80.28%, respectively, with IC_{50} values of 50.05 ± 2.16 and 1113.59 ± 29.77 µM, respectively. Furthermore, the highest inhibition percentages of the Mn(II) complex and the ligand on HeLa were 89.64 and 76.85%, respectively, with IC_{50} values of 216.35 ± 5.34 and 1198.58 ± 31.87µM, respectively. The results showed that the most sensitive cell line to the treatment was HepG-2 with the inhibition percentages of the complex and the ligand equal to 96.83 and 91.06%, respectively. The IC_{50} values were 31.11 ± 2.04 and 671.47 ± 21.41µM for the complex and the ligand, respectively (Table S2). Obviously, the cytotoxic effect was enhanced by the presence of the metal ion, the polarity of which decreased upon chelation, and the delocalization of the π-electrons increased over the whole coordination sphere, promoting the lipophilicity of the Mn(II) complex. Moreover, as the lipophilicity increased the permeation of the metal chelate to the cell membrane increased through its lipid layer [39].

For the MCF-7 and HepG-2 cell lines, which exhibited intrinsic resistance to *cis*-platin, the IC_{50} values of the reference drug were of 80 [40] and 63 µM [41], respectively, while the $[Mn(MBPT)Br(H_2O)_2]ClO_4$ complex recorded a better response with an IC_{50} value equal to 50.05 ± 2.16 µM. In addition, the anticancer activity of the Mn(II) complex was compared to the Co(II) complexes' activities against the MCF-7 cell line of the same ligand (MBPT).The IC_{50} values of complexes **2**–**5** were 439.27 ± 19.76, 438.79 ± 19.17, 674.40 ± 30.85, and 431.23 ± 20.28 µM, respectively [28], where the Mn(II) complex had the highest efficacy among them (Figure 9).

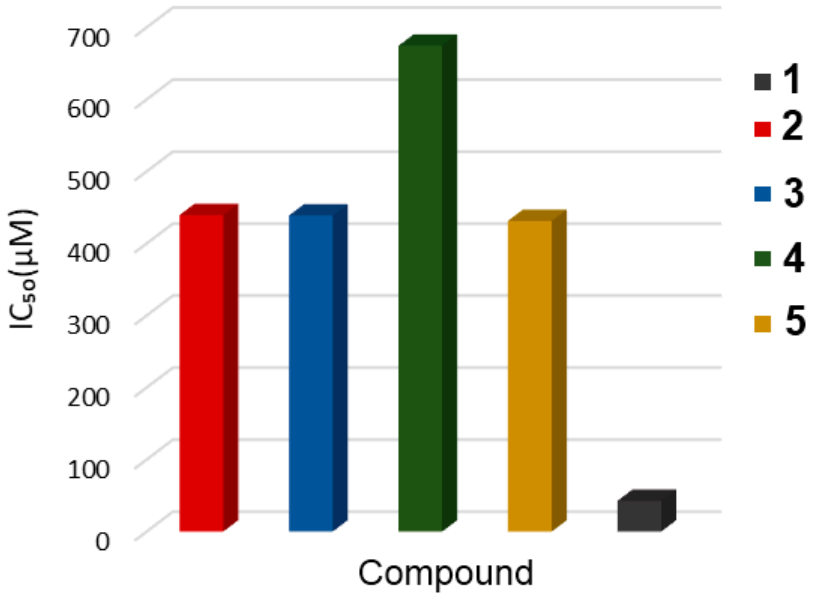

Figure 9. Anticancer activity expressed by IC_{50} values (μM) of different metal complexes against MCF-7 cell line.

3. Materials and Methods

3.1. Materials and Physical Characterization

All the details about the materials and physical characterization are described in Supplementary Data.

3.2. Synthesis

The method described by our research team was used to prepare the MBPT pincer ligand [25].

Synthesis of the $[Mn(MBPT)(H_2O)_2Br]ClO_4$ Complex

A solution of $Mn(ClO_4)_2$ (25.4 mg, 0.1 mmol) in 10 mL EtOH was mixed with 10 mL hot ethanolic solution of MBPT (29.9 mg, 0.1 mmol). Then, 1 mL of KBr aqueous solution (11.9 mg, 0.1 mmol) was added to the resulting mixture. A clear mixture was obtained which was able to slowly evaporate at R.T. Colorless crystals were formed after three days and subsequently collected through filtration. These crystals were found to be appropriate for single crystal X–ray diffraction analysis.

The yield was as follows: 87%; Anal. Calc. $C_{14}H_{21}N_7O_7MnClBr$: C, 29.52; H, 3.72; N, 17.21 and Mn, 9.64%. The following were found: C, 29.41; H, 3.77; N, 17.13 and Mn, 9.70%. The values for $[Mn(MBPT)(H_2O)_2Br]ClO_4$ FTIR cm^{-1} were as follows: 3418, 1614, 1514, 1488, 1360, 1223, 1084, 1037, 978, 756 and 629 (Figure S1).

3.3. Crystal Structure Determination

The procedures mentioned in Method S1 (Supplementary Data) describe the crystal structure determination of the studied complex [42–46]. The details of the crystal data and structural refinements are given in Table 5. In addition, Crystal Explorer 17.5 software [47] was applied to carry out the Hirshfeld calculations [48] for molecular packing analysis.

Table 5. Crystal data for $[Mn(MBPT)Br(H_2O)_2]ClO_4$.

CCDC	2155139
Empirical formula	$C_{14}H_{21}N_7O_7MnClBr$
F.Wt	569.68 g/mol
T	296(2) K
λ	0.71073 Å
Crystal system	Monoclinic
Space group	$P2_1$
Unit cell dimensions	a = 8.3217(4) Å
	b = 33.3369(16) Å
	c = 8.2814(4) Å
	β = 97.981(2)°
V	2275.17(19) Å^3
Z	4
ρ_{calc}.	1.663 g/cm^3
μ	2.503 mm^{-1}
2Θ range	5.092 to 56.54°
Reflections collected	42,472
Independent reflections	5596 [R_{int} = 0.0671, R_{sigma} = 0.0520]
Goodness-of-fit on F^2	1.12
Final R indexes [I ≥ 2σ (I)]	R_1 [a] = 0.0774, wR_2 [b] = 0.1820
Final R indexes (all data)	R_1 [a] = 0.1024, wR_2 [b] = 0.1930
Largest diff. peak and hole	1.38 and −1.31 e Å^{-3}

[a] $R_1 = \Sigma||F_o| - |F_c||/\Sigma|F_o|$. [b] $wR_2 = \{\Sigma[w(F_o^2 - F_c^2)^2]/\Sigma[w(F_o^2)^2]\}^{1/2}$.

3.4. Biological Studies

Using the protocol outlined in Method S2 (Supplementary Materials), the antimicrobial activities of the studied complex and its free ligand against various microbes were examined [49]. Furthermore, by applying Methods S3 and S4, the safety assay and anticancer activities were evaluated. Finally, the antioxidant activities were examined via Method S5 [50–53].

3.5. Computational Studies

The interaction energies of the $[Mn(MBPT)Br(H_2O)_2]^+$ complex were calculated based on the X-ray structure of the $[Mn(MBPT)Br(H_2O)_2]ClO_4$ using Gaussian 09 software [54]. The ωB97XD [55] method was used for this task. The 6-311G(d,p) basis sets were used for all the atoms except Mn (LANL2DZ).

4. Conclusions

The synthesis of $[Mn(MBPT)Br(H_2O)_2]ClO_4$ was afforded by mixing a *bis*-pyrazol-methoxy-*s*-triazine pincer ligand (MBPT) and $Mn(ClO_4)_2$/KBr in water–ethanol solution. The reaction yielded a hexa-coordinated Mn(II) complex which comprised a tridentate N-chelator ligand (MBPT), two water molecules and one bromide ion, as revealed by single-crystal X-ray structure analysis. A Hirshfeld analysis showed that H. . .H (42.8%), O. . .H (23.4%), and Br. . .H (10.6%) were the predominant interactions in the crystal structure. Also, it revealed the presence of anion–π interactions between C(*s*-triazine) and O(perchlorate) with 2.4% of the whole interactions. The M(II)-MBPT affinities were explained in terms of the metal ion size and the nature of the other coordinating ligand groups. The $[Mn(MBPT)Br(H_2O)_2]ClO_4$ complex had improved antioxidant, antibacterial and anticancer activities compared to the free ligand. The anticancer results showed high efficacy for the Mn(II) complex against HepG-2 and MCF-7 cell lines. Also, the Mn(II) complex had good activity against *S. aureus* and *B. subtilis*, and *P. vulgaris*.

Supplementary Materials: The following supporting information can be downloaded at https://www.mdpi.com/article/10.3390/inorganics12110284/s1, Experimental details; Figure S1. FTIR spectra of the ligand MBPT (A) and $[Mn(MBPT)(H_2O)_2Br]ClO_4$ complex (B); Figure S2. DPPH radical scavenging activity of Mn(II) complex, free ligand (MBPT) and ascorbic acid; Figure S3. Safety assay of $[Mn(MBPT)Br(H_2O)_2]ClO_4$ and MBPT on the non-cancerous WI-38 cell line; Table S1. Zone of Inhibition (mm) for the $[Mn(MBPT)Br(H_2O)_2]ClO_4$; Table S2. IC_{50} values (μM) of the studied systems; Method S1. Crystal structure determination; Method S2. Evaluation of antimicrobial activity; Method S3. Safety assay protocol; Method S4. Evaluation of cytotoxicity activity; Method S5. Evaluation of DPPH Radical Scavenging Activity.

Author Contributions: S.M.K.: methodology, investigation, data curation, formal analysis, validation, writing—original draft and writing—review and editing. M.S.A.: resources, software, funding, validation and data curation. A.E.-F.: conceptualization, supervision, investigation, formal analysis, resources, writing—original draft and writing—review and editing. A.B.: resources, software, validation, data curation, writing—original draft, reviewing and editing. M.H.: software, validation, data curation, writing—original draft, reviewing and editing. M.A.M.A.-Y.: conceptualization, supervision, supervision, investigation, software, formal analysis, methodology, validation, data curation, writing—original draft and writing—review and editing. S.M.S.: conceptualization, supervision, investigation, software, formal analysis, methodology, validation, data curation, writing—original draft and writing—review and editing. All authors have read and agreed to the published version of the manuscript.

Funding: Princess Nourah bint Abdulrahman University Researchers Supporting Project number (PNURSP2024R86), Princess Nourah bint Abdulrahman University, Riyadh, Saudi Arabia.

Data Availability Statement: The original contributions presented in the study are included in the article and Supplementary Materials, further inquiries can be directed to the corresponding authors.

Acknowledgments: Princess Nourah bint Abdulrahman University Researchers Supporting Project number (PNURSP2024R86), Princess Nourah bint Abdulrahman University, Riyadh, Saudi Arabia.

Conflicts of Interest: The authors declare no conflicts of interest.

References

1. Cieslik, P.; Comba, P.; Dittmar, B.; Ndiaye, D.; Tóth, É.; Velmurugan, G.; Wadepohl, H. Exceptional manganese (II) stability and manganese (II)/zinc (II) selectivity with rigid polydentate ligands. *Angew. Chem.* **2022**, *134*, e202115580. [CrossRef]
2. Sigel, A.; Sigel, R.K.; Sigel, H. *Metal Ions in Life Sciences*; Wiley: Chichester, UK, 2006; Volume 1.
3. Metzler-Nolte, N.; Kraatz, H. *Concepts and Models in Bioinorganic Chemistry*; Wiley-VCH: Chichester, UK, 2006.
4. Aschner, J.L.; Aschner, M. Nutritional aspects of manganese homeostasis. *Mol. Asp. Med.* **2005**, *26*, 353–362. [CrossRef] [PubMed]
5. Kalaiselvan, C.R.; Laha, S.S.; Somvanshi, S.B.; Tabish, T.A.; Thorat, N.D.; Sahu, N.K. Manganese ferrite ($MnFe_2O_4$) nanostructures for cancer theranostics. *Coord. Chem. Rev.* **2022**, *473*, 214809. [CrossRef]
6. Ding, B.; Shao, S.; Jiang, F.; Dang, P.; Sun, C.; Huang, S.; Ma, P.a.; Jin, D.; Kheraif, A.A.A.; Lin, J. MnO_2-disguised upconversion hybrid nanocomposite: An ideal architecture for tumor microenvironment-triggered UCL/MR bioimaging and enhanced chemodynamic therapy. *Chem. Mat.* **2019**, *31*, 2651–2660. [CrossRef]
7. Drahoš, B.; Lukeš, I.; Tóth, É. Manganese (II) complexes as potential contrast agents for MRI. *Eur. J. Inorg. Chem.* **2012**, *2012*, 1975–1986. [CrossRef]
8. Gupta, A.; Caravan, P.; Price, W.S.; Platas-Iglesias, C.; Gale, E.M. Applications for transition-metal chemistry in contrast-enhanced magnetic resonance imaging. *Inorg. Chem.* **2020**, *59*, 6648–6678. [CrossRef]
9. Roy, S.; Gu, J.; Xia, W.; Mi, C.; Guo, B. Advancements in manganese complex-based MRI agents: Innovations, design strategies, and future directions. *Drug Discov. Today* **2024**, *29*, 104101. [CrossRef]
10. Deng, Q.; Liu, J.; Li, Q.; Chen, K.; Liu, Z.; Shen, Y.; Niu, P.; Yang, Y.; Zou, Y.; Yang, X. Interaction of occupational manganese exposure and alcohol drinking aggravates the increase of liver enzyme concentrations from a cross-sectional study in China. *Environ. Health* **2013**, *12*, 30. [CrossRef]
11. Barnese, K.; Gralla, E.B.; Valentine, J.S.; Cabelli, D.E. Biologically relevant mechanism for catalytic superoxide removal by simple manganese compounds. *Proc. Natl. Acad. Sci. USA* **2012**, *109*, 6892–6897. [CrossRef]
12. Chen, P.; Chakraborty, S.; Mukhopadhyay, S.; Lee, E.; Paoliello, M.M.; Bowman, A.B.; Aschner, M. Manganese homeostasis in the nervous system. *J. Neurochem.* **2015**, *134*, 601–610. [CrossRef]
13. Senft, L.; Moore, J.L.; Franke, A.; Fisher, K.R.; Scheitler, A.; Zahl, A.; Puchta, R.; Fehn, D.; Ison, S.; Sader, S. Quinol-containing ligands enable high superoxide dismutase activity by modulating coordination number, charge, oxidation states and stability of manganese complexes throughout redox cycling. *Chem. Sci.* **2021**, *12*, 10483–10500. [CrossRef] [PubMed]

14. Dasmahapatra, U.; Maiti, B.; Alam, M.M.; Chanda, K. Anti-cancer Property and DNA Binding Interaction of First Row Transition Metal Complexes: A Decade Update. *Eur. J. Med. Chem.* **2024**, *275*, 116603. [CrossRef] [PubMed]
15. Finney, L.A.; O'Halloran, T.V. Transition metal speciation in the cell: Insights from the chemistry of metal ion receptors. *Science* **2003**, *300*, 931–936. [CrossRef] [PubMed]
16. Zhang, C.X.; Lippard, S.J. New metal complexes as potential therapeutics. *Curr. Opin. Chem. Biol.* **2003**, *7*, 481–489. [CrossRef] [PubMed]
17. Ganguly, O.M.; Moulik, S. Interactions of Mn complexes with DNA: The relevance of therapeutic applications towards cancer treatment. *Dalton Trans.* **2023**, *52*, 10639–10656. [CrossRef]
18. Dai, Q.; Sun, Q.; Ouyang, X.; Liu, J.; Jin, L.; Liu, A.; He, B.; Fan, T.; Jiang, Y. Antitumor activity of s-triazine derivatives: A systematic review. *Molecules* **2023**, *28*, 4278. [CrossRef]
19. Ali, M.I.; Naseer, M.M. Recent biological applications of heterocyclic hybrids containing s-triazine scaffold. *RSC Adv.* **2023**, *13*, 30462–30490. [CrossRef]
20. Fang, Y.; Hillman, A.S.; Fox, J.M. Advances in the Synthesis of Bioorthogonal Reagents: S-Tetrazines, 1,2,4-Triazines, Cyclooctynes, Heterocycloheptynes, and *trans*-Cyclooctenes. *Top. Curr. Chem.* **2024**, *382*, 1–63. [CrossRef]
21. Shawish, I.; Barakat, A.; Aldalbahi, A.; Malebari, A.M.; Nafie, M.S.; Bekhit, A.A.; Albohy, A.; Khan, A.; Ul-Haq, Z.; Haukka, M. Synthesis and antiproliferative activity of a new series of mono-and bis (dimethylpyrazolyl)-s-triazine derivatives targeting EGFR/PI3K/AKT/mTOR signaling cascades. *ACS Omega* **2022**, *7*, 24858–24870. [CrossRef]
22. Nehra, B.; Rulhania, S.; Jaswal, S.; Kumar, B.; Singh, G.; Monga, V. Recent advancements in the development of bioactive pyrazoline derivatives. *Eur. J. Med. Chem.* **2020**, *205*, 112666. [CrossRef]
23. Murahari, M.; Mahajan, V.; Neeladri, S.; Kumar, M.S.; Mayur, Y. Ligand based design and synthesis of pyrazole based derivatives as selective COX-2 inhibitors. *Bioorg. Chem.* **2019**, *86*, 583–597. [CrossRef] [PubMed]
24. Boro, M.; Baishya, T.; Frontera, A.; Barceló-Oliver, M.; Bhattacharyya, M.K. Energetic Features of H-Bonded and π-Stacked Assemblies in Pyrazole-Based Coordination Compounds of Mn(II) and Cu(II): Experimental and Theoretical Studies. *Crystals* **2024**, *14*, 318. [CrossRef]
25. Soliman, S.M.; El-Faham, A. Synthesis, characterization, and structural studies of two heteroleptic Mn (II) complexes with tridentate N, N, N-pincer type ligand. *J. Coord. Chem.* **2018**, *71*, 2373–2388. [CrossRef]
26. Soliman, S.M.; Almarhoon, Z.; Sholkamy, E.N.; El-Faham, A. Bis-pyrazolyl-s-triazine Ni (II) pincer complexes as selective gram positive antibacterial agents; synthesis, structural and antimicrobial studies. *J. Mol. Struct.* **2019**, *1195*, 315–322. [CrossRef]
27. Refaat, H.M.; Alotaibi, A.A.; Dege, N.; El-Faham, A.; Soliman, S.M. Synthesis, Structure and biological evaluations of Zn (II) pincer complexes based on s-triazine type chelator. *Molecules* **2022**, *27*, 3625. [CrossRef]
28. Refaat, H.M.; Alotaibi, A.A.; Dege, N.; El-Faham, A.; Soliman, S.M. Co (II) complexes based on the bis-pyrazol-s-triazine pincer ligand: Synthesis, X-ray structure studies, and cytotoxic evaluation. *Crystals* **2022**, *12*, 741. [CrossRef]
29. Sundaraganesan, N.; Ilakiamani, S.; Subramani, P.; Joshua, B.D. Comparison of experimental and ab initio HF and DFT vibrational spectra of benzimidazole. *Spectrochim. Acta A Mol. Biomol. Spectrosc.* **2007**, *67*, 628–635. [CrossRef]
30. Abuzeid, H.R.; EL-Mahdy, A.F.; Ahmed, M.M.; Kuo, S.-W. Triazine-functionalized covalent benzoxazine framework for direct synthesis of N-doped microporous carbon. *Polym. Chem.* **2019**, *10*, 6010–6020. [CrossRef]
31. Pascal, J.-L.; Potier, J.; Zhang, C.S. Chlorine trioxide, Cl_2O_6, a most efficient perchlorating reagent in new syntheses of anhydrous metal perchlorates, chloryl and nitryl perchloratometalates of cobalt (II), nickel (II), and copper (II). Reactivity of chlorine trioxide with anhydrous or hydrated chlorides and nitrates. *J. Chem. Soc. Dalton Trans.* **1985**, 297–305. [CrossRef]
32. Pascal, J.-L.; Favier, F. Inorganic perchlorato complexes. *Coord. Chem. Rev.* **1998**, *178*, 865–902. [CrossRef]
33. Pascal, J.; Potier, J.; Jones, D.; Roziere, J.; Michalowicz, A. Structural approach to the behavior of perchlorate as a ligand in transition-metal complexes using EXAFS, IR and Raman spectroscopy. 1. A perchlorate-bridged copper chain with short copper-copper distances in copper (II) perchlorate. *Inorg. Chem.* **1984**, *23*, 2068–2073. [CrossRef]
34. Hathaway, B.J. Oxyanions. *Compr. Coord. Chem.* **1987**, *1*, 413–434.
35. Soliman, S.M.; El-Faham, A. Synthesis, molecular structure and DFT studies of two heteroleptic nickel(II) s-triazine pincer type complexes. *J. Mol. Struct.* **2019**, *1185*, 461–468. [CrossRef]
36. Akila, E.; Usharani, M.; Rajavel, R. Metal (II) complexes of bioinorganic and medicinal relevance: Antibacterial, Antioxidant and DNA cleavage studies of tetradentate complexes involving O, N-donor environment of 3 3′-dihydroxybenzidine-based Schiff bases. *Int. J. Pharm. Pharm. Sci.* **2013**, *5*, 573–581.
37. Parekh, J.; Inamdhar, P.; Nair, R.; Baluja, S.; Chanda, S. Synthesis and antibacterial activity of some Schiff bases derived from 4-aminobenzoic acid. *J. Serb. Chem. Soc.* **2005**, *70*, 1155–1162. [CrossRef]
38. Shelke, V.; Jadhav, S.; Patharkar, V.; Shankarwar, S.; Munde, A.; Chondhekar, T. Synthesis, spectroscopic characterization and thermal studies of some rare earth metal complexes of unsymmetrical tetradentate Schiff base ligand. *Arab. J. Chem.* **2012**, *5*, 501–507. [CrossRef]
39. Alias, M.; Kassum, H.; Shakir, C. Synthesis, physical characterization and biological evaluation of Schiff base M (II) complexes. *J. Assoc. Arab Univ. Basic Appl. Sci.* **2014**, *15*, 28–34. [CrossRef]
40. Yde, C.W.; Issinger, O.-G. Enhancing cisplatin sensitivity in MCF-7 human breast cancer cells by down-regulation of Bcl-2 and cyclin D1. *Int. J. Oncol.* **2006**, *29*, 1397–1404. [CrossRef]

41. Gad, S.I.; Altowyan, M.S.; Abu-Youssef, M.A.; El-Faham, A.; Barakat, A.; Tatikonda, R.; Haukka, M.; Soliman, S.M.; Yousri, A. Synthesis, Structural Investigations, and Potential Antimicrobial and Anticancer Activity of Mononuclear Zn (II) and Cd (II) Complexes Decorated by Morpholine/Pyrazole s-Triazine Ligand. *Appl. Organomet. Chem.* **2024**, e7772. [CrossRef]
42. Sheldrick, G.M. SHELXT–Integrated space-group and crystal-structure determination. *Acta Crystallogr. A Found. Adv.* **2015**, *71*, 3–8. [CrossRef]
43. Sheldrick, G.M. Crystal structure refinement with SHELXL. *Acta Crystallogr. C Struct. Chem.* **2015**, *71*, 3–8. [CrossRef] [PubMed]
44. Farrugia, L.J. WinGX and ORTEP for Windows: An update. *J. Appl. Crystallogr.* **2012**, *45*, 849–854. [CrossRef]
45. *Bruker APEX2, SAINT, SADABS, and XSHELL, Bruker*; AXS Inc.: Madison, WI, USA, 2013.
46. Macrae, C.F.; Sovago, I.; Cottrell, S.J.; Galek, P.T.; McCabe, P.; Pidcock, E.; Platings, M.; Shields, G.P.; Stevens, J.S.; Towler, M. Mercury 4.0: From visualization to analysis, design and prediction. *J. Appl. Crystallogr.* **2020**, *53*, 226–235. [CrossRef] [PubMed]
47. Hirshfeld, F.L. Bonded-atom fragments for describing molecular charge densities. *Theor. Chim. Acta* **1977**, *44*, 129–138. [CrossRef]
48. Mackenzie, C.F.; Spackman, P.R.; Jayatilaka, D.; Spackman, M.A. CrystalExplorer model energies and energy frameworks: Extension to metal coordination compounds, organic salts, solvates and open-shell systems. *IUCrJ* **2017**, *4*, 575–587. [CrossRef]
49. Wayne, P. *CLSI Document M100-S22*; Performance Standards for Antimicrobial Susceptibility Testing. Twentieth Informational Supplement; Clinical and Laboratory Standards Institute (CLSI): Berwyn, PA, USA, 2012.
50. Mosmann, T. Rapid colorimetric assay for cellular growth and survival: Application to proliferation and cytotoxicity assays. *J. Immunol. Methods* **1983**, *65*, 55–63. [CrossRef]
51. Riyadh, S.M.; Gomha, S.M.; Mahmmoud, E.A.; Elaasser, M.M. Synthesis and anticancer activities of thiazoles, 1, 3-thiazines, and thiazolidine using chitosan-grafted-poly (vinylpyridine) as basic catalyst. *Heterocycles* **2015**, *91*, 1227. [CrossRef]
52. Abdelsalam, E.A.; Abd El-Hafeez, A.A.; Eldehna, W.M.; El Hassab, M.A.; Marzouk, H.M.M.; Elaasser, M.M.; Abou Taleb, N.A.; Amin, K.M.; Abdel-Aziz, H.A.; Ghosh, P. Discovery of novel thiazolyl-pyrazolines as dual EGFR and VEGFR-2 inhibitors endowed with in vitro antitumor activity towards non-small lung cancer. *J. Enzym. Inhib. Med. Chem.* **2022**, *37*, 2265–2282. [CrossRef]
53. Yen, G.C.; Duh, P.D. Scavenging effect of methanolic extracts of peanut hulls on free-radical and active-oxygen species. *J. Agric. Food Chem.* **1994**, *42*, 629–632. [CrossRef]
54. Frisch, M. *Gaussian 09, Revision d. 01*; Gaussian Inc.: Wallingford, CT, USA, 2009; Volume 201.
55. Chai, J.-D.; Head-Gordon, M. Long-range corrected hybrid density functionals with damped atom–atom dispersion corrections. *Phys. Chem. Chem. Phys.* **2008**, *10*, 6615–6620. [CrossRef]